Progress In Electromagnetics Research, Vol. 127, 189–210, 2012

AN EXTENDED DELAY-RATIONAL MACROMODEL FOR ELECTROMAGNETIC INTERFERENCE ANALYSIS OF MIXED SIGNAL CIRCUITS

M. Luo* **and K. Huang**

College of Electronics and Information Engineering, Sichuan University, Chengdu 610064, China

Abstract—This paper presents an extended delay-rational macromodel for electromagnetic interference analysis of mixed signal circuits. Firstly, an S-parameter matrix based delay-rational macromodel of the associated microwave network or system is established. Then, we extend the macromodel to include the external electromagnetic interference effects. The forced waves induced by the excitation fields are computed using full-wave method and treated as additional equivalent sources. Next, the macromodel is modified to embed the additional sources at each corresponding port. Finally, the resulting macromodel is converted into equivalent circuit for circuit analysis with the corresponding linear and non-linear port terminations. Several examples are computed by using the proposed method and the numerical results are compared with those obtained by 3-D FDTD method only. They are all in a good agreement that validate this method.

1. INTRODUCTION

With the rapidly increasing operating frequencies, circuit densities and complexity of electromagnetic environment, the external incident field or radiation efficiency of conducting traces can seriously limit the overall performance of electronic system. If not considered during early design stages, the interference can cause logic glitches or distort an analog signal that makes it fail to meet the required specifications. So, accurate prediction of the electromagnetic interference (EMI) is important for validation of electronic systems.

Various techniques have been proposed to analyze these EMI coupling problems. The first one is based on transmission line

Received 24 February 2012, Accepted 2 April 2012, Scheduled 13 April 2012

* Corresponding author: Ming Luo (mingheroluo@tom.com).

equations with quasi-TEM approximations [1–5]. This technique is preferred due to its simplicity and efficiency, but it is only suited for simple structures and low frequencies. The second is based on the full-wave solution [6–11] which successfully overcomes the shortcomings of the quasi-TEM approach. But the 3D full-wave method requires large number of memories and longer computing time. In recent years, several authors have proposed the hybrid method [12–16], i.e., the co-simulation of combining the full-wave method and commercial simulation software (such as HSPICE and ADS). In these attractive methods, the field coupling effects are analyzed by full-wave technique and incorporated into the simulators for co-simulations. But [12–14] are only suitable for the case of transmission line system, and [15] can only have the frequency analysis.

Generally, the modern high-speed complex mixed signal circuits are composed of electronic components and signal transmission lines with irregular structures such as vias, bends, crossovers and connectors. The dispersive nature in the structures requires a representation in a frequency domain, while the circuit components, especially for nonlinear ones, are ready to be formulated in the time domain. The traditional modeling and simulators do not realize this mixed domain problem [17]. Thus, the macromodeling technique [17–21] is developed. It characterizes the complex and difficult networks using an approximate but fairly accurate rational transfer function, which can be converted into an equivalent circuit model in circuit simulator. For the structures that are electrically small at the highest frequency of interesting, the vector fitting method (VFM), in its various implementations, is the standard macromodeling tool [22, 23]. When dealing with the electrical large system, this technique requires a large order of approximation and may lead to serious accuracy degradation in system-level simulation. Recently, the delay-based macromodeling techniques [24–28] are developed for more general electrical large networks. Their models include the propagation delay terms mixed with suitable rational coefficients. However, most of the macromodeling techniques are only used for signal integrity analysis and the EMI effects are not considered in these models. In [29], a hybrid method based on Krylov-space technique including EM modules is given. But, the network is represented by the admittance (Y) parameters which can cause slow convergence due to the mismatch of the terminations and lead to higher-order transfer function that increase the size of the circuit matrix. Meanwhile, it is also not suitable for analysis electrically large structure.

In this paper, we extend the delay-rational macromodel to include EMI effects by embedding the additional equivalent sources

due to external excitation fields for mixed signal circuit. The system is characterized by tabulated frequency data in the form of S-parameters and approximated by a set of delayed rational functions. Then, the finite-difference time domain method (FDTD) is used to compute the induced waves and treat them as additional sources. The delayed rational functions used to represent the port characteristics are modified to incorporate these additional sources, and subsequently realized as equivalent circuit for transient analysis with the corresponding linear and non-linear port terminations. To validate the proposed method, three examples, one microstrip line with lumped network and two circuits within a cavity all excited by external field, are studied. The results are compared with those obtained by using the 3-D FDTD method only. They are in a good agreement. This approach is fast and allows for circuit design optimization without a need for repeated analysis of the microwave network.

2. THEORY

For a typical mixed signal circuit with non-uniform structures, we introduce the N-port S-parameters network given as below to characterize it

$$\begin{bmatrix} b_1 \\ \vdots \\ b_N \end{bmatrix} = \begin{bmatrix} S_{1,1} & \cdots & S_{1,N} \\ \vdots & \ddots & \vdots \\ S_{N,1} & \cdots & S_{N,N} \end{bmatrix} \begin{bmatrix} a_1 \\ \vdots \\ a_N \end{bmatrix} \tag{1}$$

where $S_{i,j} = b_i/a_j$ with reference impedance Z_{ref_j} terminated at port j and match loads terminated at the rest. a_i and b_i are the incident and reflected waves, respectively, at the ith port. Mathematical relation between the (a_i, b_i), and voltages and currents (V_i, I_i) is given by

$$a_i = \frac{V_i + Z_{ref_i} I_i}{2\sqrt{Z_{ref_i}}}, \quad \text{and} \quad b_i = \frac{V_i - Z_{ref_i} I_i}{2\sqrt{Z_{ref_i}}} \tag{2}$$

This expression can be constructed as an interface between the circuit components and the microwave structures treated via full-wave electromagnetic fields. But, it is only applicable to modal excitations at the physical ports. Therefore, we must exploit the relation in (1) and (2) to account for non-conventional external excitations such as the external incident fields. Let us consider an external incident field impinging upon the N-port network. To account for the waves induced to the physical ports at the terminals, similar to the lumped port excitations, we treat the external field as additional sources generated

from an additional port and modify the existing N-port S-matrix as

$$\begin{bmatrix} b_1 \\ \vdots \\ b_N \end{bmatrix} = \begin{bmatrix} S_{1,1} & \dots & S_{1,N} \\ \vdots & \ddots & \vdots \\ S_{N,1} & \dots & S_{N,N} \end{bmatrix} \begin{bmatrix} a_1 \\ \vdots \\ a_N \end{bmatrix} + \begin{bmatrix} w_1^s \\ \vdots \\ w_N^s \end{bmatrix} \tag{3}$$

where w_i^s represents the additional sources due to external incident field at the ith port.

However, the frequency-domain representation in (3) can not be directly applied in the time-domain analysis. We exploit a macromodel including the external field excitations to overcome this difficult. In the subsequently subsections, we first describe the delay-rational macromodeling technique, and next, we explain how the external field excitations are computed and macromodel is extended to integrate with these additional sources.

2.1. Delay-rational Macromodel Approximation

The delay-rational function approximation aims to identify an approximation of $\mathbf{H}(s)$ from the sampled frequency S-parameters $\mathbf{S}(s)$ as shown in (1), which can be available from numerical simulation or direct measurement. Each element in $\mathbf{S}(s)$ is approximated by the delay-rational function written as

$$\begin{aligned} S_{i,j}(s) \;\cong H_{i,j}(s) &= \sum_{k=0}^{L^{i,j}-1} Q_k^{i,j}(s) e^{-s\tau_k^{i,j}} \\ &= \sum_{k=0}^{L^{i,j}-1} \left(d_k^{i,j} + \sum_{m=1}^{M_k^{i,j}} \frac{R_{k,m}^{i,j}}{s - p_{k,m}^{i,j}} \right) e^{-s\tau_k^{i,j}} \end{aligned} \tag{4}$$

where $s = j\omega$ is the Laplace variable and L the number of delay partitions in the circuit. i and j denote output and input ports, respectively, and $\tau_k^{i,j}$ represents the physical delay due to the propagation of the electromagnetic field inside the structure. For the kth part, rational coefficients $Q_k^{i,j}$ represent other effects such as attenuation and dispersion. $M_k^{i,j}$ is the total number of poles, $d_k^{i,j}$, $R_{k,m}^{i,j}$ and $p_{k,m}^{i,j}$ are the direct coupling constant, residues and poles, respectively.

Here, we must note that our analysis considers the more general electrical large networks. However, the approximation can be generalized to the cases where electronic small structures are included by removing the delay terms that is known as the standard VFM. As mentioned in Section 1, the delayed vector fitting algorithm containing

a delay estimation procedure is adopted to efficiently solve (4). This technique is briefly described as follows. (More details can be found in [26]).

The first stage is the identification of the propagation delays $\tau_k^{i,j}$ in (4) from the frequency samples $\mathbf{S}(\mathbf{s})$. This task can be accomplished by using a time-frequency decomposition provided by the so-called Gabor transform [30]. The tabulated data of $S_{i,j}(s)$ is converted to the time-frequency domain representation as

$$F_{i,j}(\omega,\tau) = \int_{-\infty}^{\infty} S_{i,j}(\zeta) W(\zeta-\omega) e^{j\zeta\tau} d\zeta \tag{5}$$

where $F_{i,j}(\omega,\tau)$ is the 2-D inverse Fourier transform function, and ω and τ are the angular frequency and time variables, respectively. $W(\zeta-\omega)$ represents a Gaussian window centered at $\zeta=\omega$ which corresponds to a Gabor transform and provides optimal support in both the time and frequency domains [30]. Then, the energy of the function $F_{i,j}(\omega,\tau)$ is calculated as

$$\eta_{i,j}(\tau) = \int_{-\infty}^{\infty} |F_{i,j}(\omega,\tau)|^2 d\omega \tag{6}$$

In the resultant energy distribution, the propagation delays will appear as sharp peaks with significant energy contributions and the delays are retained in the model by their relative contribution exceeds a predefined threshold $\delta < (\eta_{i,j}(\tau)/\sum \eta_{i,j}(\tau))$. The τ is time points. Since the neglected energy contributions are small, this procedure does not significantly affect the accuracy of the final model.

Once all propagation delays are known, the identification of poles and residues for the rational coefficients in (4) is for minimization of the linear least-squares (LS) error between the model response $\mathbf{H}(s)$ and the raw frequency samples $\mathbf{S}(s)$.

Good solution is available via a modified version of VF that uses delayed basis functions [31]. By identifying a common pole set for all delay groups, we specify a set of starting poles $\widetilde{p}_m$ in (4) and multiplies $\mathbf{S}(s)$ with an unknown function which is also approximated with the same set of starting poles $\widetilde{p}_m$. This gives the linear LS problem

$$\left(\sum_{m=1}^{M} \frac{R_m}{s-\tilde{p}_m} + 1\right) \mathbf{S}(s) = \sum_{k=0}^{L-1} \left(d_k + \sum_{m=1}^{M} \frac{R_{k,m}}{s-\tilde{p}_m}\right) e^{-s\tau_k} \tag{7}$$

Equation (7) is linear in its unknowns d_k, $R_{k,m}$, R_m and can easily be

written as

$$\sum_{k=0}^{L-1}\left(d_k+\sum_{m=1}^{M}\frac{R_{k,m}}{s-\tilde{p}_m}\right)e^{-s\tau_k}-\left(\sum_{m=1}^{M}\frac{R_m}{s-\tilde{p}_m}\right)\mathbf{S}(s)=\mathbf{S}(s) \quad (8)$$

Equation (8) leads to a linear problem, for a given frequency point s_l, we get

$$\Phi_l\chi=\Psi_l \quad (9)$$

where

$$\Phi_l=\left[1\ \ \frac{e^{-s_l\tau_0}}{s_l-\tilde{p}_1}\ \ \ldots\ \ \frac{e^{-s_l\tau_0}}{s_l-\tilde{p}_M}\ \ \ldots\ \ 1\ \ \frac{e^{-s_l\tau_{L-1}}}{s_l-\tilde{p}_1}\ \ \frac{e^{-s_l\tau_{L-1}}}{s_l-\tilde{p}_M}\ \ \frac{-S(s_l)}{s_l-\tilde{p}_1}\ \ \ldots\ \ \frac{-S(s_l)}{s_l-\tilde{p}_M}\right]$$

$$\chi=\left[\ d_0\ R_{0,1}\ldots R_{0,M}\ldots d_{L-1}\ R_{L-1,1}\ldots R_{L-1,M}\ R_1\ldots R_M\ \right]^T,$$

$$\Psi_l=S(s_l)$$

Note that Φ_l and χ are row and column vectors, respectively. After solving (9), new poles are calculated as

$$[p_m]=\mathrm{eig}\left(\Phi-\Theta\mathbf{R}^T\right) \quad (10)$$

where Θ is a column of one's and $\mathbf{R}$ a row-vector holding the residues $[R_m]$. This procedure relocates a set of initial poles to their final positions by repeated usage of (9) and (10). Finally, the unknown residues for (4) are calculated with known poles and delays.

It is noted that non-passive macromodel may lead to unstable results when used in transient simulations, even when their terminations are passive. Therefore, the model must be checked for passivity. If passivity is violated within some frequency bands, a suitable passivity enforcement process must be applied. It can be shown that the model (4) is passive if and only if [32]

$$\left(1-\mathbf{H}^H(s)\mathbf{H}(s)\right)\geq 0\quad\forall s \quad (11)$$

when all the singular values of $\mathbf{H}(s)$ do not exceed one at any frequency. If this condition is violated, passivity enforcement is mandatory. Several approaches are available [33–36] for perturbing the model coefficients in order to enforce the condition (11). All models that are used in this paper have been checked and are guaranteed passive.

2.2. Additional Sources Computation

As opposed to traditional port excitations, external incident field illumination leads to forced waves along the lines in the structure. They are not affected by the loads attached to the ports and propagate with the wave number of the incident field along the corresponding direction. Conversely, forward and backward modal waves, originated

from mismatches at ports terminations, propagate with corresponding eigenvalues that RF structure supports at the operating frequency. The inherent relation between incident, reflected and forced waves are described in (3) where forced waves are treated as additional sources at the ports. To compute the additional sources, we first update (3) to give the voltage and current relations by employing (2) as

$$[\bar{V}] - [Z_{ref}]\,[\bar{I}] = [S]\left([\bar{V}] + [Z_{ref}]\,[\bar{I}]\right) + 2\sqrt{[Z_{ref}]}\,\left[\bar{W}^s\right] \tag{12}$$

where

$$[\bar{V}] = [V_1 \ \ldots \ V_N]^T \quad [\bar{I}] = [I_1 \ \ldots \ I_N]^T \quad \left[\bar{W}^s\right] = [w_1^s \ \ldots \ w_N^s]^T$$

$$[S] = \begin{bmatrix} S_{1,1} & \ldots & S_{1,N} \\ \vdots & \ddots & \vdots \\ S_{N,1} & \ldots & S_{N,N} \end{bmatrix} \quad [Z_{ref}] = \begin{bmatrix} Z_{ref_1} & & \\ & \ddots & \\ & & Z_{ref_N} \end{bmatrix}$$

and

$$\sqrt{[Z_{ref}]} = \begin{bmatrix} \sqrt{Z_{ref_1}} & & \\ & \ddots & \\ & & \sqrt{Z_{ref_N}} \end{bmatrix}$$

The matrices $[S]$, $[Z_{ref}]$ and $\sqrt{[Z_{ref}]}$ are already known.

Then, the voltage vector and current vector are moved to the left- and right-hand sides of (12), respectively, and we can obtain

$$([U] - [S])[\bar{V}] = ([U] + [S])\,[Z_{ref}]\,[\bar{I}] + 2\sqrt{[Z_{ref}]}\,\left[\bar{W}^s\right] \tag{13}$$

where $[U]$ is a $N \times N$ identity matrix.

Rearranging the terms, an equivalent representation in terms of the impedance parameters can be written as

$$[\bar{V}] = ([U]-[S])^{-1}\,([U]+[S])\,[Z_{ref}]\,[\bar{I}] + 2([U]-[S])^{-1}\sqrt{[Z_{ref}]}\,\left[\bar{W}^s\right] \tag{14}$$

The evaluation of additional sources $[W^s]$ in (14) can now be done via open circuit analysis, in which the current $[I]$ are zeros. Thus, the additional sources are obtained as

$$\left[\bar{W}^s\right] = \frac{1}{2}\left(\sqrt{[Z_{ref}]}\right)^{-1}([U] - [S])\left[\bar{V}^{\text{open}}\right] \tag{15}$$

where $[\bar{V}^{\text{open}}]$ refers to the open circuit voltage at the ports excited by the external fields only. To find the values of the open circuit voltages, we use the FDTD analysis in which simulation is done with all ports opened. Then, the open circuit voltages at each port can be computed and recorded directly in time domain. The results at discrete time

facilitate an implementation of piecewise linear voltage sources to be incorporated into macromodel.

After calculation of the open circuit voltages, the additional sources can be obtained from (15). We substitute (15) into (3) and rewrite it as

$$[\bar{b}] = [S][\bar{a}] - \frac{1}{2}\left(\sqrt{[Z_{ref}]}\right)^{-1}[S]\left[\bar{V}^{\text{open}}\right] + \frac{1}{2}\left(\sqrt{[Z_{ref}]}\right)^{-1}\left[\bar{V}^{\text{open}}\right] \quad (16)$$

This equation can be realized as an equivalent circuit that allows a direct time-domain analysis. The process is described in the following subsection.

2.3. Macromodel Extending and Equivalent Circuit Realization

In the previous subsections, the delay-rational functions model tabulated data and additional sources computation are introduced. In order to perform a circuit simulation for the circuit including EMI effects with linear/nonlinear terminators, we derive a compact SPICE-compatible equivalent circuit stamp for the extended delay-rational macromodel from (16).

Using the delayed rational function (4), each element in (16) can be reformulated as

$$\begin{aligned} b_i(s) \;=\; & \sum_{j=1}^{N}\left\{\sum_{k=0}^{L_{i,j}-1}\left(d_k^{i,j}G_{k,m}^{i,j}(s) + \sum_{m=1}^{M_k^{i,j}} R_{k,m}^{i,j}X_{k,m}^{i,j}(s)\right)e^{-s\tau_k^{i,j}}\right\} \\ & + \frac{1}{2}\left(\sqrt{Z_{ref_i}}\right)^{-1} V_i^{\text{open}}(s) \end{aligned} \quad (17)$$

where $G_{k,m}^{i,j}(s)$ and $X_{k,m}^{i,j}$ are defined as

$$G(s) \;=\; a(s) - \frac{1}{2}\left(\sqrt{Z_{ref}}\right)^{-1} V^{\text{open}}(s) \quad (18)$$

$$X(s) \;=\; \frac{a(s) - \frac{1}{2}\left(\sqrt{Z_{ref}}\right)^{-1} V^{\text{open}}(s)}{s-p} \quad (19)$$

Then, Equations (17)–(19) can be transformed into a set of delayed state-space formulation. In the conversion, the Jordan-form state-space realization [17] and similarity transformation are used to replace the complex poles with their real and imaginary parts. The final form of the delayed state-space formulation gives

$$\begin{cases} \frac{d\mathbf{x}(t)}{dt} = \mathbf{A}\mathbf{x}(t) + \mathbf{B}\mathbf{g}(t) \\ \mathbf{b}(t) = \sum\limits_{k=0}^{L-1}\mathbf{C}_k\mathbf{x}(t-\tau_k) + \sum\limits_{k=0}^{L-1}\mathbf{D}_k\mathbf{g}(t-\tau_k) + \frac{1}{2}\left(\sqrt{\mathbf{Z}_{ref}}\right)^{-1}\mathbf{V}^{\text{open}}(t) \end{cases} \quad (20)$$

where matrices $\mathbf{A}$ is the state matrix, $\mathbf{B}$ the input mapping matrix, $\mathbf{C}_k$ the residues, and $\mathbf{D}_k$ the direct coupling constants. $\mathbf{x}(t-\tau_k)$ is the delayed state vector and $\mathbf{g}(t-\tau_k)$ the delayed input vector.

In order to illustrate the conversion of the delayed rational functions (17) to the delayed state-space formulation (20), consider a two-port example with two common poles and two common delays $\tau_1 = 0$ and $\tau_2 = \Gamma$ whose transfer function is described by (for the sake of clarity, we omit the complex frequency term s)

$$\begin{bmatrix} b_1 \\ b_2 \end{bmatrix} = \begin{bmatrix} \sum\limits_{k=0}^{1}\left(d_k^{1,1}+\sum\limits_{m=1}^{2}\frac{R_{k,m}^{1,1}}{s-p_m}\right)e^{-s\tau_k} & \sum\limits_{k=0}^{1}\left(d_k^{1,2}+\sum\limits_{m=1}^{2}\frac{R_{k,m}^{1,2}}{s-p_m}\right)e^{-s\tau_k} \\ \sum\limits_{k=0}^{1}\left(d_k^{2,1}+\sum\limits_{m=1}^{2}\frac{R_{k,m}^{2,1}}{s-p_m}\right)e^{-s\tau_k} & \sum\limits_{k=0}^{1}\left(d_k^{2,2}+\sum\limits_{m=1}^{2}\frac{R_{k,m}^{2,2}}{s-p_m}\right)e^{-s\tau_k} \end{bmatrix} \begin{bmatrix} G_1 \\ G_2 \end{bmatrix} + \begin{bmatrix} B_1 \\ B_2 \end{bmatrix} \tag{21}$$

where

$$\begin{bmatrix} G_1 \\ G_2 \end{bmatrix} = \begin{bmatrix} a_1 - \frac{1}{2}\sqrt{Z_{ref_1}}^{-1} V_1^{\text{open}} \\ a_2 - \frac{1}{2}\sqrt{Z_{ref_2}}^{-1} V_2^{\text{open}} \end{bmatrix} \text{ and } \begin{bmatrix} B_1 \\ B_2 \end{bmatrix} = \begin{bmatrix} \frac{1}{2}\sqrt{Z_{ref_1}}^{-1} V_1^{\text{open}} \\ \frac{1}{2}\sqrt{Z_{ref_2}}^{-1} V_2^{\text{open}} \end{bmatrix}$$

Let X_1, X_3, X_3 and X_4 be the state variables in the frequency-domain, and let $\{x_i\}$, $\{g_i\}$ and $\{b_i'\}$ be the time-domain equivalent of $\{X_i\}$, $\{G_i\}$ and $\{B_i\}$, respectively, such that

$$(s-p_1)X_1 = G_1 \Rightarrow \dot{x}_1(t) = p_1 x_1(t) + g_1(t) \tag{22a}$$

$$(s-p_2)X_2 = G_1 \Rightarrow \dot{x}_2(t) = p_2 x_2(t) + g_1(t) \tag{22b}$$

$$(s-p_1)X_3 = G_2 \Rightarrow \dot{x}_3(t) = p_1 x_3(t) + g_2(t) \tag{22c}$$

$$(s-p_2)X_4 = G_2 \Rightarrow \dot{x}_4(t) = p_2 x_4(t) + g_2(t) \tag{22d}$$

Substituting (22) into (21) and taking the inverse Laplace transform yields

$$\begin{aligned} \begin{bmatrix} b_1(t) \\ b_2(t) \end{bmatrix} = {} & \begin{bmatrix} R_{0,1}^{1,1} & R_{0,2}^{1,1} & R_{0,1}^{1,2} & R_{0,2}^{1,2} \\ R_{0,1}^{2,1} & R_{0,2}^{2,1} & R_{0,1}^{2,2} & R_{0,2}^{2,2} \end{bmatrix} \begin{bmatrix} x_1(t) \\ x_2(t) \\ x_3(t) \\ x_4(t) \end{bmatrix} \\ & + \begin{bmatrix} d_0^{1,1} & d_0^{1,2} \\ d_0^{2,1} & d_0^{2,2} \end{bmatrix} \begin{bmatrix} g_1(t) \\ g_2(t) \end{bmatrix} \\ & + \begin{bmatrix} R_{1,1}^{1,1} & R_{1,2}^{1,1} & R_{1,1}^{1,2} & R_{1,2}^{1,2} \\ R_{1,1}^{2,1} & R_{1,2}^{2,1} & R_{1,1}^{2,2} & R_{1,2}^{2,2} \end{bmatrix} \begin{bmatrix} x_1(t-\Gamma) \\ x_2(t-\Gamma) \\ x_3(t-\Gamma) \\ x_4(t-\Gamma) \end{bmatrix} \\ & + \begin{bmatrix} d_1^{1,1} & d_1^{1,2} \\ d_1^{2,1} & d_1^{2,2} \end{bmatrix} \begin{bmatrix} g_1(t-\Gamma) \\ g_2(t-\Gamma) \end{bmatrix} + \begin{bmatrix} b_1'(t) \\ b_2'(t) \end{bmatrix} \end{aligned} \tag{23}$$

And (22) can be written in a matrix form as

$$\begin{bmatrix} \dot{x}_1(t) \\ \dot{x}_2(t) \\ \dot{x}_3(t) \\ \dot{x}_4(t) \end{bmatrix} = \begin{bmatrix} p_1 & & & \\ & p_2 & & \\ & & p_1 & \\ & & & p_2 \end{bmatrix} \begin{bmatrix} x_1(t) \\ x_2(t) \\ x_3(t) \\ x_4(t) \end{bmatrix} + \begin{bmatrix} 1 & 0 \\ 1 & 0 \\ 0 & 1 \\ 0 & 1 \end{bmatrix} \begin{bmatrix} g_1(t) \\ g_2(t) \end{bmatrix} \quad (24)$$

Finally, (23) and (24) can be rewritten as

$$\begin{aligned} \frac{d\mathbf{x}(t)}{dt} &= \mathbf{A}\mathbf{x}(t) + \mathbf{B}\mathbf{g}(t) \\ \mathbf{b}(t) &= \sum_{k=0}^{L-1} \mathbf{C}_k \mathbf{x}(t-\tau_k) + \sum_{k=0}^{L-1} \mathbf{D}_k \mathbf{g}(t-\tau_k) + \mathbf{b}'(t) \end{aligned} \quad (25)$$

Once the delayed state-space form of (25) has been constructed, it can be converted into an equivalent circuit. Depending on the SPICE platform, we use capacitors for time derivatives, resistors and controlled sources for multiplication by constants, and matched ideal transmission lines for delay operators. As shown in Eq. (20), the additional sources due to external incident field are realized via the open circuit voltages, which are computed at discrete times and implemented as piecewise linear voltage sources incorporated into the circuit. An equivalent network representing (20) can be constructed as shown in Figure 1.

3. NUMERICAL EXAMPLES

In this section, several numerical examples are presented to demonstrate the validity and accuracy of the proposed method.

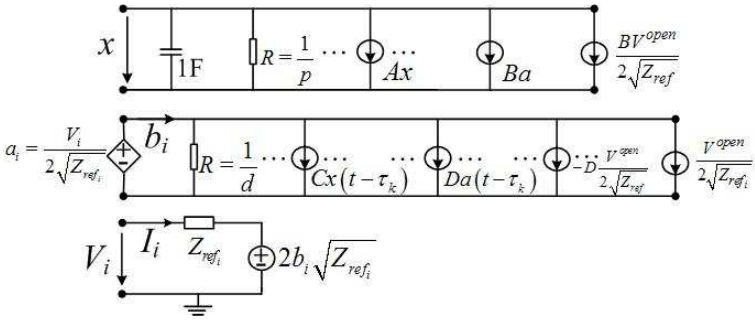

Figure 1. Equivalent circuit realization for the extended delay-rational macromodel.

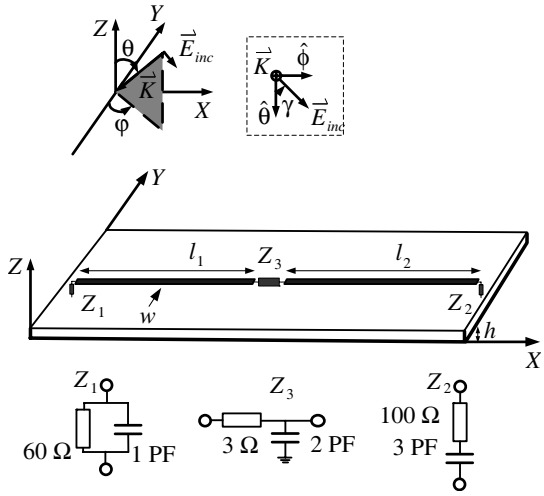

Figure 2. Schematics of a microstrip circuit. Parameter values are $l_1 = l_2 = 100\,\text{mm}$, $h = 2\,\text{mm}$, $w = 1\,\text{mm}$ and $\varepsilon_r = 2.65$.

3.1. Microstrip Circuit with Lumped-distributed Network

The first case is a circuit terminated by linear/nonlinear loads as shown in Figure 2, made of a chain of two microstrip lines with a lumped-distributed network in between. The test structure is exposed to an incident plane wave having the form of Gaussian pulse $\vec{E} = \vec{E}_0 e^{-((t-t_0)/T)^2}$ with an amplitude of $E_0 = 1\,\text{KV/m}$. The bandwidth is determined by $t_0 = 2\,\text{ns}$ and $T = 0.3\,\text{ns}$. It illuminates the circuit from the upper face with the angular parameters of $\theta = 45°$, $\varphi = 90°$ and $\gamma = 0°$.

First, the port S-parameters of the circuit is computed by the full-wave method in the frequency range of 0.1–10 GHz. Then, the delayed rational function approximation is carried out to match the S-parameters. Figure 3 compares the frequency responses of the delayed macromodel to the raw data used for the model identification. An excellent agreement between them is observed.

Subsequently, the open circuit voltages at each port are computed by using the FDTD method and used to derive the additional sources. Therefore, the equivalent circuit of the macromodel is created with these sources incorporated. The transient simulation analysis is performed using the constructed circuit and the results are given in Figure 4. As we can see, they are in a general good agreement with the results obtained by using 3-D FDTD method only.

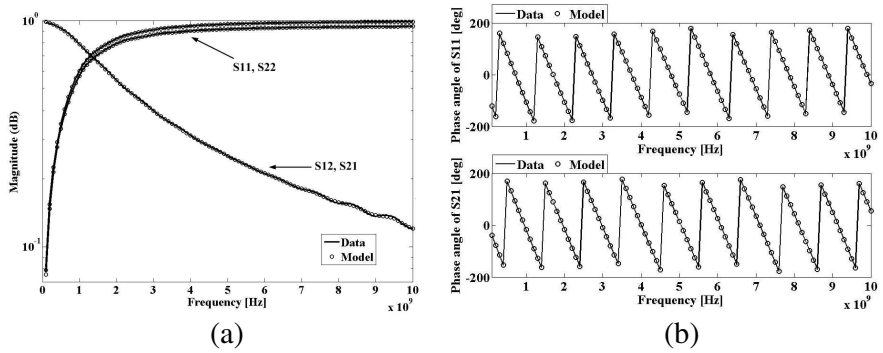

Figure 3. Comparison between the model and data for the S-parameters of the circuit. (a) Magnitude of the S-parameters, and (b) phase of the S-parameters.

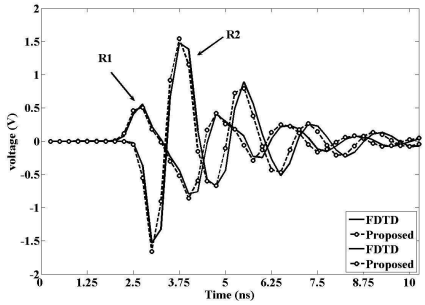

Figure 4. Transient output voltages at the two loads R_1 and R_2.

To find what will happen if the frequency is outside of the range provided by the raw data, Figure 5(a) gives the comparison between the frequency responses of the delayed rational macromodel and the S-parameters obtained by using full-wave method in the range of 0.01–20 GHz. Figure 5(b) gives the transient results of the test structure excited by a Gaussian pulse waveform with amplitude of 1 KV/m and bandwidth of 0.01–20 GHz. As we can see, most of the results are in a good agreement, and show the generalization of the model.

3.2. Printed Circuit Board inside an Enclosure

The second example is a more complex two layer printed circuit board inside an enclosure as shown in Figure 6. The enclosure with dimensions of $L_e \times W_e \times H_e$, and thickness T_e has a set of slots with

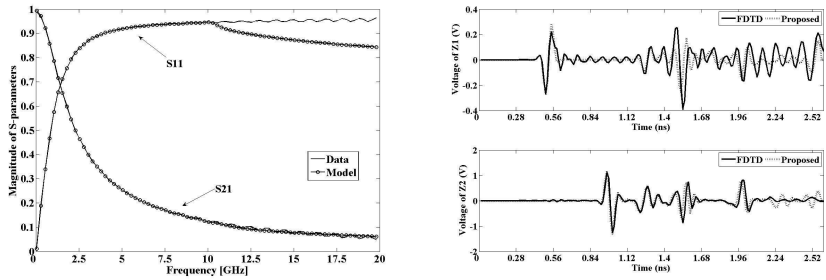

Figure 5. Responses predicted by the macromodel in a more broad frequency range. (a) The comparison of S-parameters between the mocromodel and full-wave method. (b) The comparison of the voltage responses at each load between the macromodel and FDTD method.

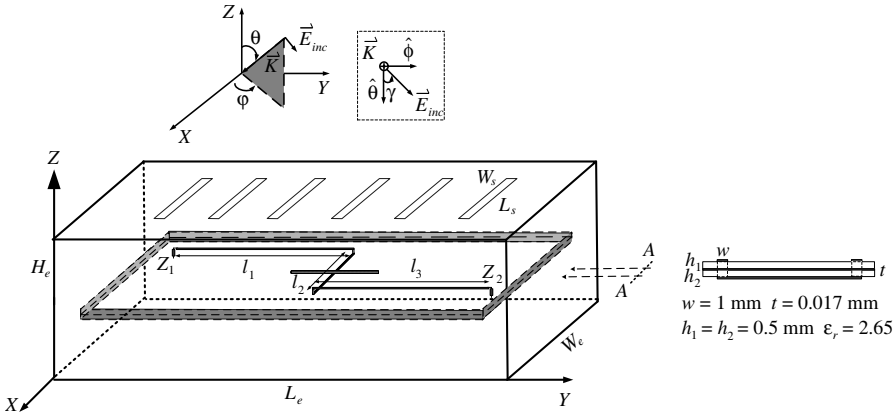

Figure 6. PCB inside the enclosure excited by external field. Parameter values are $L_e = 200\,\text{mm}$, $W_e = 120\,\text{mm}$, $H_e = 50\,\text{mm}$, $L_s = 80\,\text{mm}$, $W_s = 3\,\text{mm}$, $l_1 = l_2 = l_3 = 50\,\text{mm}$.

length L_s and width W_s on it top surface. The circuit is composed of microstrip lines with vias, and the middle metal layer is for the ground plane. There is a slot ($30\,\text{mm} \times 1\,\text{mm}$) in the ground plane which forms a discontinuity in the transmission system. The two terminal loads Z_1 and Z_2 are attached to the ports P_1 and P_2, respectively. Z_1 is a RC parallel circuit with resistance $R_1 = 30\,\Omega$ and capacitor $C_1 = 5\,\text{pF}$, Z_2 is a diode. A Gaussian pulse wave $\vec{E} = \vec{E}_0 e^{-((t-t_0)/T)^2}$ with $E_0 = 10\,\text{KV/m}$, $t_0 = 2\,\text{ns}$ and $T = 0.5\,\text{ns}$ incident to the system.

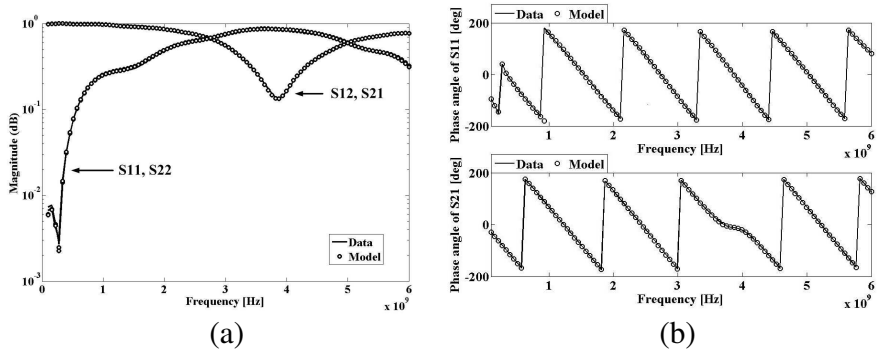

Figure 7. Comparison between the model and data for the S-parameters of the circuit. (a) Magnitude of the S-parameters, and (b) phase of the S-parameters.

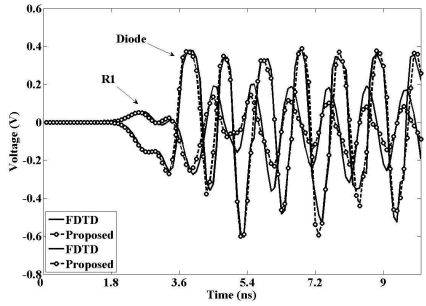

Figure 8. Transient output voltages at the two loads R_1 and R_2.

The incident angle is $\theta = 45°$, $\varphi = 45°$ and $\gamma = 45°$.

As a precious case, the delayed rational function approximation is carried out to match the S-parameters of the circuit up to 6 GHz. The approximated values from the macromodel are compared with those from the tabulated data, as shown in Figure 7. Then, the equivalent circuit is constructed from the extended delay-rational macromodel and the transient analysis is performed as shown in Figure 8. Again, it can be observed that all the results are in good agreement.

3.3. Field Coupling to PCB inside Cavity

In this example, we study field coupling to a PCB designed for RF circuit and located inside a cavity subjected to field excitation (see Figure 9). There is an aperture on the top surface of the cavity.

A Gaussian pulse wave $\vec{E} = \vec{E}_0 e^{-((t-t_0)/T)^2}$ with $E_0 = 10\,\mathrm{KV/m}$, $t_0 = 1.5\,\mathrm{ns}$ and $T = 0.3\,\mathrm{ns}$ incident to the system. The incident angle is $\theta = 45°$, $\varphi = 90°$ and $\gamma = 0°$. The external field can couple to the PCB through the aperture.

As before, we exploit the macromodel of the four-port network with additional sources incorporated for transient analysis of the EMI problem. In the simulation, Z_1 is a RL parallel circuit with resistance $R_1 = 60\,\Omega$ and $L_1 = 2\,\mathrm{nH}$ at port 1, and Z_2 is a RC parallel circuit with resistance $R_2 = 200\,\Omega$ and $C_2 = 5\,\mathrm{pF}$ at port 2. The ports 3 and 4, at Z_3 and Z_4 are opened, respectively. The transient simulation results are shown in Figure 10. They agree with the results obtained by FDTD method only that validates the proposed method.

Next, we use the established model to investigate output characteristics of a JFET amplifier circuit subjected to external

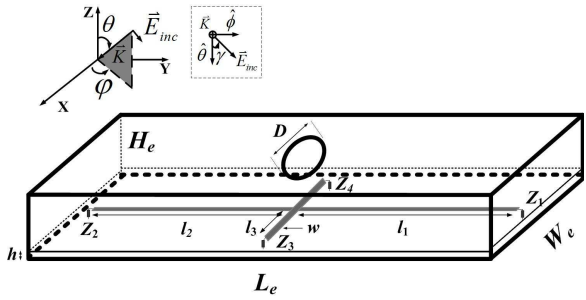

Figure 9. PCB inside cavity excited by external field. Parameter values are $L_e = 120\,\mathrm{mm}$, $W_e = 50\,\mathrm{mm}$, $H_e = 20\,\mathrm{mm}$, $L_s = 80\,\mathrm{mm}$, $w = 1\,\mathrm{mm}$, $l_1 = l_2 = 50\,\mathrm{mm}$, $l_3 = 10\,\mathrm{mm}$, $h = 2\,\mathrm{mm}$ and $D = 10\,\mathrm{mm}$.

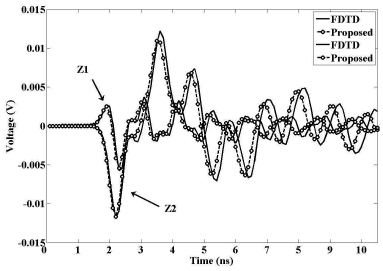

Figure 10. Transient output voltages at the two loads Z_1 and Z_2.

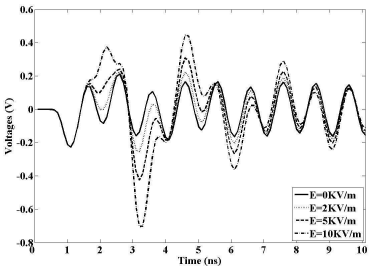

Figure 11. Transient output voltages of the amplifier in different incident field intensity.

incident field. For the circuit as shown in Figure 8, the termination Z_2 is replaced by the JFET amplifier circuit. A sinusoidal voltage source as port excitation with magnitude of 10 mV operating at 1 GHz is applied to the port 1. Figure 11 is the output voltages of the amplifier in different incident field intensity. It has been clearly see that external EMI generates deteriorating on the output of the amplifier and

Table 1. Delays estimates and number of poles comparison.

Example No.	Parameters	Delays		Order	
		τ_0	τ_1	Without Delay	With Delay
1	S_{11}	0.0 ns	0.932 ns	28	6
	S_{21}	0.925 ns	1.858 ns		
2	S_{11}	0.0 ns	0.787 ns	22	8
	S_{21}	0.79 ns	-		
3	S_{11}	0.0 ns	0.413 ns	18	8
	S_{21}	0.393 ns	0.955 ns		

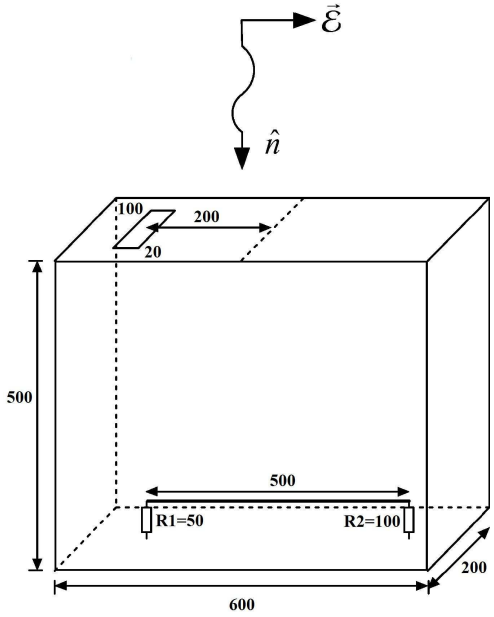

Figure 12. Lossless single line within a cavity excited by an incident field. (Unit: mm).

it becomes more dominant with increasing incident field magnitudes. Thereby, this example implies that even though the RF circuit is shielded, a small aperture cut-out for some special requirements may lead to severe coupling to the devices, and eventual system level upset.

A summary of delays estimates and the comparison of the total number of poles for each parameter in the above examples are given in Table 1. Since the S-parameters are obtained by terminating all the ports with matching loads, the delays and number of orders will be reduced. Due to the space limit, only S_{11} and S_{21} parameters are displayed in the table.

3.4. Transmission Lines in Cavity

In this subsection, to further validate the proposed method, the responses of transmission line in a cavity excited by external incident

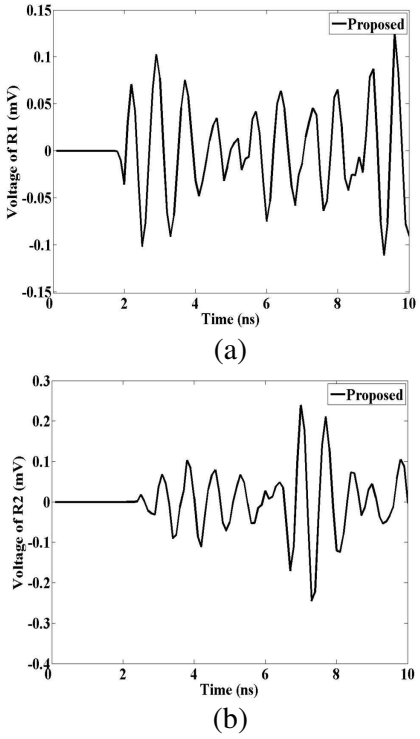

Figure 13. Transient voltages at loads. (a) Voltage of R_1. (b) Voltage of R_2.

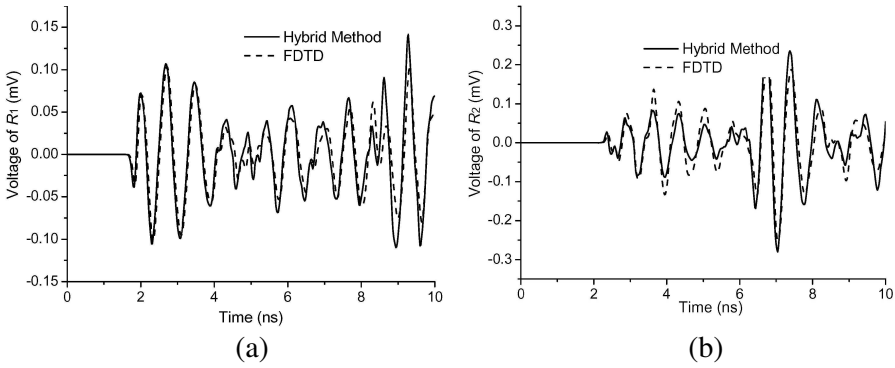

Figure 14. Transient voltages at loads in [13]. (a) Voltage of R_1. (b) Voltage of R_2.

field are compared with some existing results obtained by other works. A lossless single line inside the cavity is excited by external incident field, as shown in Figure 12. The time waveform of the incident electric field is a biexponential pulse, described by the expression $\vec{E} = e^{(-t/t_1)} - e^{(-t/t_2)}$, where t_1 and t_2 equal 0.5 and 0.2 ns, respectively. (more details can be found in [13]).

The transient voltages at the two loads by using the proposed method are shown in Figure 13. For comparison, the results given in [13] are shown in Figure 14. As we can see, they agree with each other very well. The divergences among them are mainly caused by the different distances of the incident fields applied in our method and in [13].

4. CONCLUSIONS

An extended delay-rational macromodel including EMI effects for mixed signal circuit is proposed in this paper. Through the approach, the EMI problem is downsized to a circuit analysis and provides an easy and efficient way to include the linear/nonlinear terminal devices. In addition, the proposed method is fast. Once the macromodel is generated, it can be re-used in different circuits that speed up the whole optimization process. Numerical examples are given, and good agreements are obtained comparing with other methods, which validate the accuracy of the proposed method.

ACKNOWLEDGMENT

This project is supported by the National Science Foundation of China under Grant No. 60871064.

REFERENCES

1. Bernardi, P., R. Cicchetti, and C. Pirone, "Transient response of a microstrip line circuit excited by an external electromagnetic source," *IEEE Trans. Electromagn. Compat.*, Vol. 34, No. 2, 100–108, May 1992.
2. Erdin, I., R. Khazaka, and M. Nakhla, "Simulation of high speed interconnects in multilayered medium in the presence of incidence field," *IEEE Trans. Microw. Theory Tech.*, Vol. 47, No. 12, 2251–2257, Dec. 1998.
3. Tesche, F. M., M. V. Ianoz, and T. Karlsson, *EMC Analysis Methods and Computational Models*, Wiley, New York, 1997.
4. Paul, C. R., "A SPICE model for multiconductor transmission lines excited by an incident electromagnetic field," *IEEE Trans. Electromagn. Compat.*, Vol. 36, No. 4, 342–354, Nov. 2009.
5. Pergol, M. and W. Zieniutycz, "Rectangular microstrip resonator illuminated by normal-incident plane wave," *Progress In Electromagnetics Research*, Vol. 120, 83–97, 2011.
6. Sui, W., D. A. Christensen, and C. H. Durney, "Extending the two dimensional FDTD method to hybrid electromagnetic systems with active and passive lumped elements," *IEEE Trans. Microw. Theory Tech.*, Vol. 40, No. 4, 724–730, Apr. 1992.
7. Picket-May, M., A. Taflove, and J. Baron, "FDTD modeling of digital signal propagation in 3-D circuits with passive and active loads," *IEEE Trans. Microw. Theory Tech.*, Vol. 42, No. 8, 1514–1523, Aug. 1994.
8. Leviatan, Y., E. Hudis, and P. D. Einziger, "A method of moments analysis of electromagnetic coupling through slots using a Gaussian beam expansion," *IEEE Trans. Antennas Propagat.*, Vol. 37, 1537–1544, Dec. 1989.
9. Rajamani, V., C. F. Bunting, M. D. Deshpande, and Z. A. Khan, "Validation of modal/MoM in shielding effectiveness studies of rectangular enclosures with apertures," *IEEE Trans. Electromagn. Compat.*, Vol. 48, No. 2, 348–353, May 2006.
10. Carpes, Jr., W. P., L. Pichon, and A. Razek, "Analysis of the coupling of an incident wave with a wire inside a cavity using an

FEM in frequency and time domains," *IEEE Trans. Electromagn. Compat.*, Vol. 44, No. 3, 470–475, Aug. 2002.

11. Klopf, E. M., S. B. Manić, M. M. Ilic, and B. M. Notaros, "Efficient time-domain analysis of waveguide discontinuities using higher order FEM in frequency domain," *Progress In Electromagnetics Research*, Vol. 120, 215–234, 2011.
12. Bayram, Y. and J. L. Volakis, "Hybrid *S*-parameters for transmission line networks with linear/nonlinear load terminations subject to arbitrary excitations," *IEEE Trans. Microw. Theory Tech.*, Vol. 55, No. 5, 941–950, May 2007.
13. Xie, H., J. Wang, R. Fan, and Y. Liu, "A hybrid FDTD-SPICE method for transmission lines excited by a nonuniform incident wave," *IEEE Trans. Electromagn. Compat.*, Vol. 51, No. 3, 811–817, Aug. 2009.
14. Xie, H., J. Wang, R. Fan, and Y. Liu, "Spice models for radiated and conducted susceptibility analyses of multiconductor shielded cables," *Progress In Electromagnetics Research*, Vol. 103, 241–257, 2010.
15. Yang, T., Y. Bayram, and J. L. Volakis, "Hybrid analysis of electromagnetic interference effects on microwave active circuits within cavity enclosures," *IEEE Trans. Electromagn. Compat.*, Vol. 52, No. 3, 745–748, Aug. 2010.
16. Xie, H., J. Wang, D. Sun, R. Fan, and Y. Liu, "SPICE simulation and experimental study of transmission lines with TVSs excited by EMP," *Journal of Electromagnetic Waves and Applications*, Vol. 24, Nos. 2–3, 401–411, 2010.
17. Achar, R. and M. S. Nakhla, "Simulation of high-speed interconnects," *Proceedings of the IEEE*, Vol. 89, 693–728, May 2001.
18. Watanabe, T. and H. Asai, "Synthesis of time-domain models for interconnects having 3-D structure based on FDTD method," *IEEE Trans. Circuits Syst. II*, Vol. 47, 302–305, Apr. 2000.
19. Li, E., E. X. Liu, L. W. Li, and M. S. Leong, "A coupled efficient and systematic full-wave time-domain macromodeling and circuit simulation method for signal integrity analysis of high-speed interconnects," *IEEE Trans. Advanced Packaging*, Vol. 27, No. 1, Feb. 2004.
20. Liu, E.-X. and E.-P. Li, "Finite-difference time-domain macromodel for simulation of electromagnetic interference at high-speed interconnects," *IEEE Trans. Magnetics.*, Vol. 41, No. 65–71, Jan. 2005.

21. Remis, R. F., "An efficient model-order reduction approach to low-frequency transmission line modeling," *Progress In Electromagnetics Research*, Vol. 101, 39–155, 2010.
22. Gustavsen, B. and A. Semlyen, "Rational approximation of frequency domain responses by vector fitting," *IEEE Trans. Power Delivery*, Vol. 14, 1052–1061, Jul. 1999.
23. Gustavsen, B., "Computer code for rational approximation of frequency dependent admittance matrices," *IEEE Trans. Power Delivery*, Vol. 17, 1167–1098, Oct. 2002.
24. Charest, A., D. Saraswat, M. Nakhla, R. Achar, and N. Soveiko, "Compact macromodeling of high-speed circuits via delayed rational functions," *IEEE Microw. Wireless Comp. Lett.*, Vol. 17, 828–830, Dec. 2007.
25. Charest, A., M. Nakhla, and R. Achar, "Delay extracted stable rational approximations for tabulated networks with periodic reflections," *IEEE Microw. Wireless Comp. Lett.*, Vol. 19, 768–770, Dec. 2009.
26. Chinea, A., P. Triverio, and S. Grivet-Talocia, "Delay-based macromodeling of long interconnects from frequency-domain terminal responses," *IEEE Trans. Advanced Packaging*, Vol. 33, 246–256, Feb. 2010.
27. Triverio, P., S. Grivet-Talocia, and A. Chinea, "Identification of highly efficient delay-rational macromodels of long interconnects from tabulated frequency data," *IEEE Trans. Microw. Theory Tech.*, Vol. 58, No. 3, 566–577, Mar. 2010.
28. Charest, A., M. S. Nakhla, R. Achar, D. Saraswat, N. Soveiko, and I. Erdin, "Time domain delay extraction-based macromodeling algorithm for long-delay networks," *IEEE Trans. Advanced Packaging*, Vol. 33, 219–235, Feb. 2010.
29. Erdin, I., M. S. Nakhla, and R. Achar, "Circuit analysis of electromagnetic radiation and field coupling effects for networks with embedded full-wave modules," *IEEE Trans. Electromagn. Compat.*, Vol. 42, No. 4, 449–460, Nov. 2000.
30. Yao, J. and P. Krolak, "The generalized Gabor transform," *IEEE Trans. Image Process.*, Vol. 4, 978–988, Jul. 1995.
31. Gustavsen, B. and J. Nordstrom, "Pole identification for the universal line model based on trace fitting," *IEEE Trans. Power Delivery*, Vol. 23, No. 1, Jan. 2008.
32. Cangellaris, A. C. and M. Celik, "Electromagnetic model order reduction for system-level modeling," *IEEE Trans. Microw. Theory Tech.*, Vol. 47, No. 6, 840–851, Jun. 1999.

33. Gad, E., C. Chen, M. Nakhla, and R. Achar, "Passivity verification in delay-based macromodels of electrical interconnects," *IEEE Trans. Circuits Syst. I*, Vol. 52, 2173–2187, Oct. 2005.
34. Chen, C., E. Gad, M. Nakhla, and R. Achar, "Passivity verification in delay-based macromodels of multiconductor electrical interconnects," *IEEE Trans. Advanced Packaging*, Vol. 30, 246–256, May 2007.
35. Chinea, A. and S. Grivet-Talocia, "A passivity enforcement scheme for delay-based transmission line macromodels," *IEEE Microw. Wireless Comp. Lett.*, Vol. 17, 562–564, Aug. 2007.
36. Chinea, A. and S. Grivet-Talocia, "Perturbation schemes for passivity enforcement of delay-based transmission line macromodels," *IEEE Trans. Advanced Packaging*, Vol. 31, 568–578, Aug. 2008.